Effects of uniaxial stress on excitons in Cu_2O

R. G. Waters*
Department of Physics, The City College of the City University of New York, New York, New York 10031

Fred H. Pollak
Department of Physics, Brooklyn College of the City University of New York, New York, New York 11210

R. H. Bruce† and H. Z. Cummins
Department of Physics, The City College of the City University of New York, New York, New York 10031

(Received 25 June 1979)

We have investigated the effects of uniaxial stress up to 2.5 kbar on the first four dipole-forbidden states of the yellow exciton series in cuprous oxide. The linear and nonlinear splittings and shifts as well as the symmetries of the stress-split components were determined using the quadrupole-dipole Raman-scattering technique involving odd-parity phonons. We have observed the triply degenerate 1*S* quadrupole state split into a singlet and a doublet with the singlet energy increasing and the doublet energy decreasing with stress as first seen by Gross and Kaplyanskii. For the higher quadrupole *S* states, however, the *sense* of the splitting was reversed from that of the 1*S*, while the magnitude of the 3*S* splitting exceeded that of the 1*S* as previously noted by Agekyan and Stepanov. The quadratic stress coefficients for all components of the 1*S*, 3*D*, and 4*S* states were found to be equal while those for the 3*S* state were markedly different. A theoretical analysis was carried out for [001] stress using the effective-Hamiltonian formalism including both deformation of the bands and electron-hole exchange. The theory accounts satisfactorily for the general features of the 1*S*, 3*D*, and 4*S* states only if both the magnitude and sign of the exchange constant are considered to be dependent on the exciton state. For the 3*S*, however, the nonlinear stress dependence cannot be reconciled with the theory for yellow excitons. These results suggest that the "3*S* yellow exciton" may actually belong to the green-exciton series, or that interactions between yellow and green excitons with different principal quantum numbers may be significant although not included in the theory.

INTRODUCTION

Excitons in Cu_2O have been studied extensively since their discovery nearly 30 years ago.[1] Excitons of the fundamental (yellow) series are both very sharp and difficult to observe as a result of the direct forbidden bandgap. Yellow *P* states are weakly dipole allowed, and eight or more members of the *P* series can be observed in good crystals in absorption or luminescence. Yellow *S* states, however, are strictly dipole-forbidden.

The 1*S* yellow state was first observed in weak electric quadrupole absorption by Gross and Kaplyanskii in 1960.[2] Quadrupole transitions to higher *S* states are masked by phonon-assisted absorption to the 1*S* state and are usually studied by applying a symmetry-breaking perturbation to the crystal. The currently accepted level assignments for excited yellow *S* and *D* states are derived from electroabsorption and electroreflection measurements, largely due to Nikitine and co-workers.[3,4]

Uniaxial stress measurements have played an important role in the study of excitons in Cu_2O. Gross and Kaplyanskii's observations in 1960[5] of the polarization of the stress-split components of the 1*S* yellow state established its quadrupole character and provided the experimental basis for Elliott's 1961 band assignments.[6] The applied stress in these experiments did not exceed 1 kbar and the splittings were observed to be linear in the stress. Although stress splitting of some weak absorption features was observed by Agekyan, Gross, and Kaplyanskii in 1965,[7] the weakness of the absorption precluded detailed analysis. In 1975, Agekyan and Stepanov again investigated the stress splitting of excited *S* states, but with the addition of a static electric field.[8] The observed dependence of the stress splitting on principal quantum number led them to question the accepted energy-level assignments and to propose a new classification scheme for the yellow excition states. However, they were unable to establish the symmetries of the stress-split excited states because of the admixture of *P* states produced by the static electric field.

We have previously reported[9] the observation of forbidden resonant Raman scattering in Cu_2O in which strong scattering from normally-Raman-forbidden odd-parity phonons is observed when the incident laser light is tuned to resonance with a quadrupole absorption. This effect can be exploited as a "quadrupole spectrometer" since there is a strong enhancement of the Raman cross-section as the laser is scanned through quadrupole (but not dipole) exciton states without the appli-

cation of additional symmetry-breaking perturbations.

In this communication we present the results of forbidden-resonant-Raman-scattering spectroscopy of Cu_2O subjected to uniaxial stress. We have measured splittings of several states in both the linear and nonlinear stress regions, and have also established the symmetries of the stress-split components.

EXPERIMENT

Experiments were performed at ~4 °K on a Cu_2O crystal cut from a large boule grown by Brower and Parker using the floating zone technique.[10] The crystal was mounted in a stress apparatus which is described elsewhere[11] and placed in a Janis "supervaritemp" dewar. All spectra were obtained with a Coherent Radiation model 590 dye laser pumped by a Spectra Physics model 165 argon-ion laser. Scattered light was analyzed using a Spex 1401 double-grating spectrometer and photon counting electronics and was recorded on a strip chart recorder. The dye laser output was passed through a Spex minimate spectrometer before reaching the sample to reduce the broadband dye fluorescence. Stepping motors were connected to the tuning drives of the dye laser and the minimate spectrometer which allowed these instruments to be frequency scanned electronically.

The Cu_2O sample was cut as a parallelepiped ($2 \times 2 \times 10$ mm) with the [100] directions as principal axes. The surfaces of the crystal were mechanically polished and etched with concentrated HNO_3. Backscattering measurements could be made from a (100) surface with stress applied perpendicular to the scattering plane along [001]. Measurements were made with about 40 mW of dye laser power, which caused no detectable heating of the sample.

Laser tuning was accomplished in a series of discrete steps of about 3 cm^{-1} each until resonant enhancement of the Γ_3^- (109 cm^{-1}) phonon had commenced. At this point, the tuning increments were reduced to ~1 cm^{-1}. The Raman intensity was measured at each incident frequency until the laser was well away from resonance. The measurements were repeated as stress was applied to the crystal. The effect of the stress was to produce a splitting and/or shift in the resonant frequency. This behavior presumably corresponds to the effect of stress on the exciton states themselves. Once a splitting had been observed, the Raman intensity was studied as a function of incident and scattered polarization with the laser tuned to resonance with each of the stress-split exciton states in turn. All combinations of incident

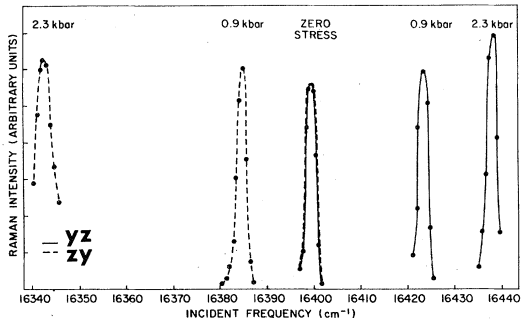

FIG. 1. Raman intensity for the Γ_3^- 109-cm^{-1} phonon vs incident laser frequency for incident frequencies near the 1*S* state of the yellow exciton in Cu_2O. The results for two finite stresses are shown as well as the zero-stress case. The occurrence of pairs of resonant peaks for a given stress is evident. The polarization configuration in which an enhancement occurs is denoted by *yz* (solid line) or *zy* (dashed line) where the first (second) letter corresponds to the incident (scattered) polarization vector. The direction denoted by *z* is parallel to the applied stress while *y* is perpendicular to both the stress and the propagation direction of the incident light.

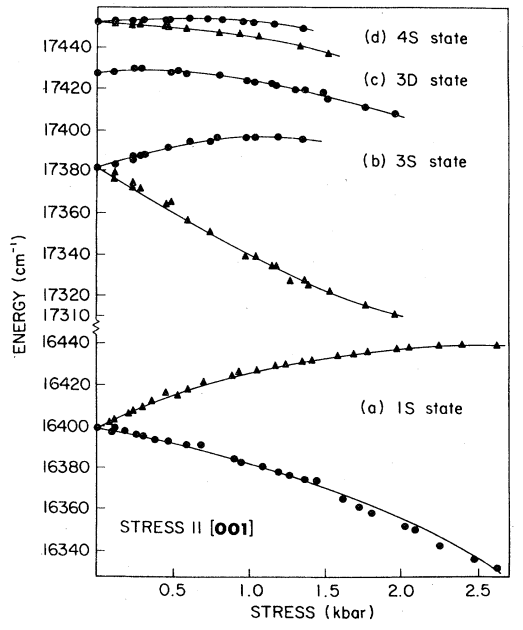

FIG. 2. Energy of resonant Raman-scattering maxima vs applied stress in Cu_2O for tetragonal stress. The data points give the energy of quadrupole-allowed ($^3\Gamma_5^+$) exciton states. Polarization selection rules allow identification of the doubly degenerate ($^2\Gamma_5^+$) and nondegenerate ($^1\Gamma_4^+$) levels into which the states split under stress. Where a splitting occurs, these are indicated by circles and triangles, respectively. No splitting is resolved for the 3*D* state.

and scattered polarizations parallel and perpendicular to the stress direction were studied. Comparison of the results with group theory predictions enabled us to determine the symmetry and degeneracy of the excition state responsible for each resonance.

Raman intensity as a function of incident frequency with the laser tuned through the region of the 1S state of the yellow excition is shown in Fig. 1. We have exhibited the results for the unstressed crystal as well as for two finite stresses. Figure 2 is a plot of the frequencies at which the peak of the resonance enhancement occurs versus applied stress. The degeneracy of exciton states is also indicated. The magnitude of the splittings (~100 cm^{-1} for the 1S state) and the nonlinear behavior will be discussed below.

THEORY

The ${}^3\Gamma_5^+$ valence band of Cu_2O, derived from Cu(3d) orbitals in spin-orbit split into ${}^2\Gamma_7^+$ (upper) and ${}^4\Gamma_8^+$ (lower) valence bands. The ${}^1\Gamma_1^+$ conduction band with spin becomes ${}^2\Gamma_6^+$. Yellow excitons are formed from a ${}^2\Gamma_7^+$ hole and ${}^2\Gamma_6^+$ electron, while green excitons are formed from a ${}^4\Gamma_8^+$ hole and ${}^2\Gamma_6^+$ electron. The four 1S states of the yellow excition (${}^2\Gamma_7^+ \otimes {}^2\Gamma_6^+$) are further split by exchange into a ${}^1\Gamma_2^+$ and ${}^3\Gamma_5^+$. The ${}^1\Gamma_2^+$ paraexciton is forbidden in both electric dipole and electric quadrupole optical transitions. Several recent experiments have placed it approximately 100 cm^{-1} below the ${}^3\Gamma_5^+$.[12,14]

The ${}^3\Gamma_5^+$ orthoexciton transforms under O_h as xy, yz, and zx. Thus for light incident along $\hat{x}$, it can be excited by both y and z polarizations. Under a uniaxial stress along $\hat{z}$, the crystal symmetry is lowered to D_{4h}, and the ${}^3\Gamma_5^+$ orthoexciton separates into ${}^1\Gamma_4^+$ and ${}^2\Gamma_5^+$. Since these transform as, respectively, (xy) and (yz, zx) the ${}^1\Gamma_4^+$ state can be excited by y polarization and the ${}^2\Gamma_5^+$ by z polarization. A full calculation by R. Berenson,[15] following the analysis for unstressed crystals by J. Birman,[16] of the selection rules for quadrupole–dipole scattering from the Γ_3^- (109 cm^{-1}) phonon shows that the ${}^1\Gamma_4^+$ state can participate only in (yz) polarization and the ${}^2\Gamma_5^+$ only in (zy). We have made explicit use of these selection rules in identifying the symmetries of the stress-split components in Fig. 1. A summary of the effects of tetragonal strain on states of electric quadrupole and electric dipole symmetry as well as on the Γ_3^- phonon (which can mediate transitions between these) is given in Table I.

Since the valence and conduction bands forming the yellow exciton are both Kramer's doublets, the observed linear splitting with stress cannot arise from simple deformation splitting of the bands. Rather, it is a second-order effect involving the simultaneous effects of exchange and strain, as first noted by Elliott.[6] The theory of exchange-strain splitting has been discussed by a number of authors,[11] including Kiselev and Zhilich,[17] who have worked out much of the theory for Cu_2O.

We have carried out a calculation of the exchange-strain splitting in Cu_2O, following the approaches of Kiselev and Zhilich, of Langer, Euwema, Era, and Koda,[18] and of Cho[19] based on the effective Hamiltonian formalism of Pikus.[20]

The starting point for the calculation is the effective-mass approximation in which excition wave functions are given by

$$\Psi = \Phi_n(r_e - r_h)\Psi_v(r_h)\Psi_c(r_e), \tag{1}$$

i.e., an envelope function Φ of the relative electron-hole motion multiplying a pair of zone-center Bloch band functions.

Since the conduction band is an orbital singlet (Γ_1^+) times a spin doublet (Γ_6^+), there are two possible conduction states $\Psi_c = \alpha_c$ or β_c, (spin up or down), multiplying a totally symmetric spatial part which we will not explicitly include. The valence band is an orbital triplet Γ_5^+ transforming as xz, yz, or xy times a spin doublet (α or β) giving six valence states and thus, when combined with the two conduction states, 12 pair states of the form

$$\Psi_v\Psi_c = [xy(\alpha)](\beta_c), \text{ etc.} \tag{2}$$

The 12 basis functions to be used in the calculation are linear combinations of the simple product functions of Eq. (2) chosen both to diagonalize the major part of the perturbation in the unstrained crystal and to exhibit the appropriate symmetries of the yellow and green excitons.

The transformation is accomplished in two steps. First, the six valence functions $\Psi_v = xy\alpha$, etc., are combined to form two Γ_7 and four Γ_8 basis functions using the coefficients (coupling constants) given in Koster *et al.*[21] Since these functions transform as representations of the appropriate double group, they automatically diagonalize the spin-orbit interaction.[22] The six valence functions are given in the Appendix in Table V both in Cartesian coordinates and in spherical harmonics. Next, the four "yellow" product functions formed from the two Γ_7^+ valence states and the conduction α_c or β_c are combined into four new product functions, one transforming as Γ_2^+ and three as Γ_5^+, which are then the appropriate functions for the exchange-split para and ortho yellow excitions. Similarly, the eight "green" product functions formed from the four Γ_8^+ valence states and the conduction α_c or β_c are

TABLE I. Transformation properties of operators and phonons involved in quadrupole-dipole Raman scattering in unstressed (cubic) and uniaxially stressed (tetragonal) Cu_2O. Square brackets indicate coordinate combinations which transform according to the representations indicated. Parentheses indicate polarization of incident and scattered light.

	O_h	D_{4h}
Electric quadrupole operator	$^3\Gamma_5^+$ $[xy, yz, zx]$	$^1\Gamma_4^+$ $[xy]$
		$^2\Gamma_5^+$ $[xz, yz]$
Electric dipole operator	$^3\Gamma_4^-$ $[x, y, z]$	$^1\Gamma_2^-$ $[z]$
		$^2\Gamma_5^-$ $[x, y]$
109-cm^{-1} phonon	$^2\Gamma_3^-$	$^1\Gamma_1^-$
		$^1\Gamma_3^-$
Reduction of direct product for quadrupole-dipole process	$^3\Gamma_5^+ \otimes {}^3\Gamma_4^- = {}^1\Gamma_2^- + {}^2\Gamma_3^- + {}^3\Gamma_4^- + {}^3\Gamma_5^-$	$^2\Gamma_5^+ \otimes {}^1\Gamma_2^- = {}^2\Gamma_5^-$
		$^1\Gamma_4^+ \otimes {}^2\Gamma_5^- = {}^2\Gamma_5^-$
		$^2\Gamma_5^+ \otimes {}^2\Gamma_5^- = {}^1\Gamma_1^- + {}^1\Gamma_2^- + {}^1\Gamma_3^- + {}^1\Gamma_4^-$
		$^1\Gamma_4^+ \otimes {}^1\Gamma_2^- = {}^1\Gamma_3^-$
Polarization selection rules for participation of 109-cm^{-1} phonon (Ref. 15)	$x(yz)\bar{x}$	$x(zy)\bar{x}$ for $^2\Gamma_5^+$ exciton
	$x(zy)\bar{x}$	$x(yz)\bar{x}$ for $^1\Gamma_4^+$ exciton

combined into eight new functions transforming as a double Γ_3^+, a triplet Γ_4^+, and a triplet Γ_5^+. The appropriate coefficients are again taken from Koster *et al.*[21]

These 12 product basis functions are diagonal in the spin-orbit interaction, and the four yellow and eight green functions are separately diagonal in the exchange interaction as well, although interseries exchange terms will remain. The 12 functions including envelope functions Φ are listed in Table VI. For a given orbital quantum state n(e.g., $n=1S$) there will be two distinct envelope functions Φ_{ny} and Φ_{ng} for the yellow and green excitons, respectively, as indicated in the table. The sequence $(\phi_1, \ldots, \phi_{12})$ has been chosen for convenience to block diagonalize the final energy matrix.

The initial Hamiltonian H_0 includes the spin-orbit interaction $H_{so}=\frac{2}{3}\Delta\vec{L}\cdot\vec{\sigma}$ which splits the valence band into Γ_7^+ and Γ_8^+ (with Γ_8^+ lying below Γ_7^+ by the spin-orbit energy Δ), and the Coulomb energy E_c^{gn} and E_c^{yn} for the green and yellow excitons, respectively. Thus, the energy E_0 for the 12 basis states without strain or exchange will be $E_0=E_c^{yn}$ for the four yellow exciton states and $E_c^{gn}+\Delta$ for the eight green exciton states. These are also listed in Table VI.

The effective exciton Hamiltonian is $H=H_0+H_1$, where

$$H_1=H_D+H_{ex}.$$

H_D describes the effects of deformation on the valence and conduction bands and H_{ex} represents the electron-hole exchange interaction. The deformation Hamiltonian for the O_h point group is[11,23]

$$H_D=a\,\mathrm{Tr}\epsilon-3b[(L_z^2-\tfrac{1}{3}L^2)\epsilon_{zz}+\text{c.p.}]-2d\sqrt{3}\,(\{L_yL_z\}\epsilon_{yz}+\text{c.p.}), \quad (3)$$

where ϵ_{ij} are components of the strain tensor, L_y and L_z are angular-momentum operators, a, b, and d are deformation potentials, c.p. are cyclic permutations, and $\{L_yL_z\}$ is the anticommutator $[L_yL_z+L_zL_y]$. For the case of tetragonal stress, this becomes

$$H_D=a(S_{11}+2S_{12})X-3b(S_{11}-S_{12})(L_z^2-\tfrac{1}{3}L^2)X \equiv hX+e(L_z^2-\tfrac{1}{3}L^2)X, \quad (4)$$

where the S_{ij} are elastic compliance constants, X is the applied stress, and h and e are deformation parameters defined here for convenience. The first term in Eq. (4) represents the effect of the hydrostatic component of the strain on the band gap while the second term produces the strain splitting of the orbitally degenerate $^4\Gamma_8^+$ valence band as well as band mixing effects.

The exchange part of the Hamiltonian can be

written as

$$H_{ex} = \tfrac{1}{2} F J^A \vec{\sigma}_e \cdot \vec{\sigma}_h , \tag{5}$$

where J^A is an atomic exchange constant, $\vec{\sigma}_e$ and $\vec{\sigma}_h$ operate on conduction electron and valence hole spin functions, respectively, and F is a factor which gives the probability that the electron and hole are in the same cell:

$$F = |\Phi(0)|^2 .$$

The exchange interaction $\frac{1}{2}FJ^A$ will depend both on the valence band involved and on the principal quantum number n of the exciton state, because $|\Phi(r_e - r_h = 0)|^2 \sim n^{-3}$. For a given n, the matrix elements of H_{ex} are

$$\langle \phi_i | H_{ex} | \phi_j \rangle = \tfrac{1}{2} J_{ij} \langle i | \vec{\sigma}_e \cdot \vec{\sigma}_h | j \rangle ,$$

where $\langle i|$ and $|j\rangle$ refer to the spin part of the wave functions in Table VI and J_{ij} is[19]:

$$\begin{aligned} J_{yy} &= J_y^A |\Phi_{ny}(0)|^2 \equiv J_y , \\ J_{gg} &= J_g^A |\Phi_{ng}(0)|^2 \equiv J_G , \\ J_{yg} &= \sqrt{J_y^A J_g^A}\,[\Phi_{ny}^*(0)\Phi_{ng}(0)] \equiv J . \end{aligned} \tag{6}$$

The matrix of the effective Hamiltonian in the 12-state basis of Table VI is given in Table II. In computing the matrix elements of the deformation potential H_D, envelope function factors of the form $\int \Phi_i^* \Phi_j d^3r$ occur. For yellow-yellow or green-greeen matrix elements these are equal to unity by definition. For matrix elements between yellow and green states they turn out to be nearly equal to unity as well and thus have not been included explicitly in Table II.

Several aspects of the energy matrix should be noted:

(1) The exchange interaction is very nearly diagonal. The only off-diagonal terms are between yellow and green Γ_5 excitons of the same symmetry ($G\Gamma_{yz}^5$ and $Y\Gamma_{yz}^5$; $G\Gamma_{xz}^5$ and $Y\Gamma_{xz}^5$; $G\Gamma_{xy}^5$ and $Y\Gamma_{xy}^5$).

(2) The sole effect of the hydrostatic deformation term hX is to shift all the diagonal energies linearly.

(3) Terms linear in eX occur in the diagonal elements of the green excitons giving rise to linear splitting due to splitting of the Γ_8 valence band. However, no such terms occur in the energies of the yellow excitons (E_5, E_8, E_{10}, E_{12}) showing that these states are not split by the strain to first order. Splittings must therefore come about in second order due to the off-diagonal matrix elements of eX between yellow and green states.

(4) The matrix includes only yellow and green excitons of a particular orbital quantum state (e.g., $3S$). No interactions between states of different quantum numbers have been included, nor have possible interactions with other valence or conduction bands, such as the blue or violet exciton series.

The Hamiltonian matrix can be diagonalized numerically for different values of the parameters and compared directly with the experimental data. However, it is useful first to solve approximately for the energy eigenvalues using second-order perturbation theory:

$$E_n = H_{0,nn} + H_{1,nn} + \sum_{k \neq n} \frac{|H_{nk}|^2}{E_{0n} - E_{0k}} . \tag{7}$$

Since ϕ_3 and ϕ_4 are degenerate in H_0, the exchange part of H_1 has also been included in the energy denominator for this pair (i.e., $E_{03} - E_{04} = 4J_g/3$) and similarly for ϕ_6 and ϕ_7.

Finally, the yellow Coulomb energy E_c^y was subtracted from the resulting energy eigenvalues and the combination $\Delta + E_c^g - E_c^y$ represented by Δ' (which now depends on the particular exciton state). The final energies shown in Table III are thus measured from the energy of the specific yellow exciton without exchange and strain.

Note that the yellow triplet orthoexcition is predicted to split into a doublet and a singlet under applied uniaxial stress. The linear splitting comes from the cross term in the squared off-diagonal matrix element $(4J/3\sqrt{2} + eX/\sqrt{2})^2$ and is thus seen to arise from the simultaneous effects of exchange and strain as stated earlier.

COMPARISON OF EXPERIMENT AND THEORY

The second-order perturbation approximation results of the preceding theoretical analysis, summarised in Table III, predict that S states of the yellow triplet orthoexciton series should be split by tetragonal stress into a doublet and a singlet whose energies, relative to their zero stress values, are

$$\begin{aligned} E_{\text{doublet}}(X) &= hX - (4eJ/3\Delta')X - (2e^2/\Delta')X^2 , \\ E_{\text{singlet}}(X) &= hX + (8eJ/3\Delta')X - (2e^2/\Delta')X^2 . \end{aligned} \tag{8}$$

The experimental data shown in Fig. 2 were least-squares fit to the function $E = C_1X + C_2X^2$ and the resulting linear and quadratic coefficients are listed in Table IV. (The doublet and singlet were distinguished experimentally by polarization selection as indicated in Table I.) The state assignments follow those of the Strasbourg group with the $3D_1$ assumed to be partially quadrupole through hybridization with the nearby $4S$.[3,4]

Comparison of the data with Eqs. (8) is complicated by the n dependence of Δ', which is not directly measurable since the energies of the green S exciton states are uncertain. A reasonable approximation to $\Delta'(n)$ is obtained by taking the difference of the energies given by the Rydberg equations for the p states[3,9]

TABLE II. Matrix of the effective Hamiltonian $H=H^0+H^1$ in the 12-state basis of Table VI.

$H^0=\Delta+E_c$, $H^1=\frac{1}{2}J_{ij}\vec{\sigma}_e\cdot\vec{\sigma}_h+hX+e(L_z^2-\frac{1}{3}L^2)X$.

	ϕ_1 $(G\Gamma_z^4)$	ϕ_2 $(G\Gamma_1^3)$	ϕ_3 $(G\Gamma_x^4)$	ϕ_4 $(G\Gamma_{yz}^5)$	ϕ_5 $(Y\Gamma_{yz}^5)$	ϕ_6 $(G\Gamma_y^4)$	ϕ_7 $(G\Gamma_{xz}^5)$	ϕ_8 $(Y\Gamma_{xz}^5)$	ϕ_9 $(G\Gamma_{xy}^5)$	ϕ_{10} $(Y\Gamma_{xz}^5)$	ϕ_{11} $(G\Gamma_2^3)$	ϕ_{12} $(Y\Gamma^2)$
ϕ_1	$\Delta+E_c^G+\frac{1}{2}J_G+hX-eX$	0	0	0	0	0	0	0	0	0	0	0
ϕ_2	0	$\Delta+E_c^G+\frac{1}{2}J_G+hX-eX$	0	0	0	0	0	0	0	0	0	0
ϕ_3	0	0	$\Delta+E_c^G+\frac{1}{2}J_G+hX+\frac{1}{2}eX$	$-\frac{\sqrt{3}}{2}eX$	$-(\frac{3}{2})^{1/2}eX$	0	0	0	0	0	0	0
ϕ_4	0	0	$-\frac{\sqrt{3}}{2}eX$	$\Delta+E_c^G-\frac{5}{6}J_G+hX-\frac{1}{2}eX$	$\frac{4J}{3\sqrt{2}}+\frac{eX}{\sqrt{2}}$	0	0	0	0	0	0	0
ϕ_5	0	0	$-(\frac{3}{2})^{1/2}eX$	$\frac{4J}{3\sqrt{2}}+\frac{eX}{\sqrt{2}}$	$E_c^y-\frac{1}{6}J_y+hX$	0	0	0	0	0	0	0
ϕ_6	0	0	0	0	0	$\Delta+E_c^G+\frac{1}{2}J_G+hX+\frac{1}{2}eX$	$\frac{\sqrt{3}}{2}eX$	$(\frac{3}{2})^{1/2}eX$	0	0	0	0
ϕ_7	0	0	0	0	0	$\frac{\sqrt{3}}{2}eX$	$\Delta+E_c^G-\frac{5}{6}J_G+hX-\frac{1}{2}eX$	$\frac{4}{3\sqrt{2}}J+\frac{e}{\sqrt{2}}X$	0	0	0	0
ϕ_8	0	0	0	0	0	$(\frac{3}{2})^{1/2}eX$	$\frac{4}{3\sqrt{2}}J+\frac{e}{\sqrt{2}}X$	$E_c^y-\frac{1}{6}J_y+hX$	0	0	0	0
ϕ_9	0	0	0	0	0	0	0	0	$\Delta+E_c^G-\frac{5}{6}J_G+hX+eX$	$\frac{4}{3\sqrt{2}}J-e\sqrt{2}X$	0	0
ϕ_{10}	0	0	0	0	0	0	0	0	$\frac{4}{3\sqrt{2}}J-e\sqrt{2}X$	$E_c^y-\frac{1}{6}J_y+hX$	0	0
ϕ_{11}	0	0	0	0	0	0	0	0	0	0	$\Delta+E_c^G+\frac{1}{2}J_G+hX+eX$	$-\sqrt{2}eX$
ϕ_{12}	0	0	0	0	0	0	0	0	0	0	$-\sqrt{2}eX$	$E_c^y+\frac{1}{2}J_y+hX$

TABLE III. Eigenvalues of the energy matrix (Table II) from second-order perturbation theory.

Yellow Γ_5 triplet orthoexciton

$$\phi_5\,(Y\Gamma^5_{yz}),\ \phi_8\,(Y\Gamma^5_{xz}):\quad E_5=E_8=\left(-\frac{1}{6}J_y-\frac{8}{9}\frac{J^2}{\Delta'}\right)+hX-\frac{4eJ}{3\Delta'}X-\frac{2e^2}{\Delta'}X^2$$

$$\phi_{10}\,(Y\Gamma^5_{xy}):\quad E_{10}=\left(-\frac{1}{6}J_y-\frac{8}{9}\frac{J^2}{\Delta'}\right)+hX+\frac{8eJ}{3\Delta'}X-\frac{2e^2}{\Delta'}X^2$$

Yellow Γ_2 singlet paraexciton

$$\phi_{12}\,(Y\Gamma^2):\quad E_{12}=(+\tfrac{1}{2}J_y)+hX-\frac{2e^2}{\Delta'}X^2$$

Green Γ_5 triplet

$$\phi_7\,(G\Gamma^5_{xz}),\ \phi_4\,(G\Gamma^5_{yz}):\quad E_7=E_4=\left(\Delta'-\frac{5}{6}J_G+\frac{8J^2}{9\Delta'}\right)+hX+\left(\frac{4J}{3\Delta'}-\frac{1}{2}\right)eX+\left(\frac{1}{2\Delta'}-\frac{9}{16J_G}\right)e^2X^2$$

$$\phi_9\,(G\Gamma^5_{xy}):\quad E_9=\left(\Delta'-\frac{5}{6}J_G+\frac{8J^2}{9\Delta}\right)+hX-\left(\frac{8J}{3\Delta'}-1\right)eX+\frac{2e^2}{\Delta'}X^2$$

Green Γ_4 triplet

$$\phi_3\,[G\Gamma^4_x],\ \phi_6\,(G\Gamma^4_y):\quad E_3=E_6=(\Delta'+\tfrac{1}{2}J_G)+hX+\frac{e}{2}X+\left(\frac{9}{16J_G}+\frac{3}{2\Delta'}\right)e^2X^2$$

$$\phi_1\,(G\Gamma^4_z):\quad E_1=(\Delta'+\tfrac{1}{2}J_G)+hX-eX$$

Green Γ_3 doublet

$$\phi_2\,(G\Gamma^3_1):\quad E_2=(\Delta'+\tfrac{1}{2}J_G)+hX-eX$$

$$\phi_{11}\,(G\Gamma^3_2):\quad E_{11}=(\Delta'+\tfrac{1}{2}J_G)+hX+eX+\frac{2e^2}{\Delta'}X^2$$

$$E_g=18\,588-1242/n^2\ \text{cm}^{-1},\qquad E_y=17\,523-795/n^2\ \text{cm}^{-1},\tag{9}$$

and assuming that the central cell corrections and/or quantum defects which shift S states relative to these values will be similar for the yellow and green series. The resulting Δ' is 618 cm^{-1} for $n=1$ and increases monotonically with n towards the ionization limit $\Delta'(\infty)=1065$ cm^{-1}, which is just the spin-orbit energy Δ. These values of $\Delta'(n)$ are also listed in Table IV.

Since Δ' is positive for all n and $J\propto n^{-3}$ while the deformation parameters h and e are assumed to be independent of n, the sense of the linear splitting is predicted by Eqs. (8) to be the same for all yellow exciton states, while its magnitude should decrease faster than n^{-3}. This prediction is seen to be in clear disagreement with the data since the sense of the splitting of the $1S$ state (singlet moves up, doublet moves down) is inverted in the higher states. Furthermore, the magnitude of the splitting is larger for $3S$ than for $1S$, as previously noted by Agekyan and Stepanov.[8]

Equations (8) also predict that the quadratic coefficient C_2 should be negative for all states, with equal magnitude for the doublet and singlet of a given n, and should decrease with increasing n as $1/\Delta'$. Although the $1S$, $3D$, and $4S$ states exhibit negative and approximately equal values of C_2, the $3S$ state is again seen to behave anomalously. (The positive curvature of the $3S$ $^1\Gamma_4^+$ is also evident in the data of Fig. 2.)

In view of the errors inherent in the perturbation approximation, further analysis was performed by diagonalization of the energy matrix (Table II) for a sequence of values of the stress in the range 0 to 2.75 Kbar. The diagonalization was performed as a subroutine of a nonlinear least-squares fitting program which varies the parameters Δ', J, e, and h to produce a best fit of the predicted yellow exciton energies $E_{5,8}$ and E_{10} to the experimental values. First, however, the number of independent exchange constants was reduced from three to one.

The three exchange parameters J, J_y, and J_g which appear in the energy matrix (Table II) are related by Eqs. (6). The atomic exchange factors J_y^A and J_g^A may be different since the Bloch functions may involve somewhat different distributions within the unit cell. Neglecting this effect which should in any case be small, one has only the difference in $|\Phi(0)|^2$ which is proportional to $(\mathcal{R}/n)^3$, where $\mathcal{R}$ is the Rydberg constant and n is the principal quantum number. Since the ratio

TABLE IV. Computer analysis of experimental stress-dependent exciton energies.

Exciton state (Strasbourg notation)	Δ' (cm^{-1}) (estimated)	Polynomial fit: $E = C_1X + C_2X^2$ C_1 (cm^{-1} $kbar^{-1}$)	C_2 (cm^{-1} $kbar^{-2}$)
$1S$ $^1\Gamma_4^+$	618	+31.4 ±0.1	−6.5 ±0.1
$^2\Gamma_5^+$		−11.4 ±0.1	−6.2 ±0.1
$3S$ $^1\Gamma_4^+$	1015	−50.5 ±1.4	+6.3 ±0.8
$^2\Gamma_5^+$		+28.2 ±1.9	−12.8 ±1.2
$3D$	(1015)	+0.33 ±1.5	−5.7 ±0.7
$4S$ $^1\Gamma_4^+$	1037	−1.64 ±2.2	−4.9 ±1.5
$^2\Gamma_5^+$		+7.73 ±1.2	−6.8 ±1.2

Matrix diagonalization

		J (cm^{-1})	e (cm^{-1} $kbar^{-1}$)	h (cm^{-1} $kbar^{-1}$)	a (eV)	b (eV)
$1S$	(Δ' = 600 cm^{-1})	−183	47	−4	−1.8	−0.3
	(Δ' = 3600 cm^{-1})	−357	123	−5	−2.1	−0.8
CuCl [a]						−0.4

[a] Reference 26.

of green to yellow Rydberg constants [Eq. (9)] is very close to $4^{1/3}$, we then have:

$$J = J_0/n^3,$$
$$J_y = \tfrac{1}{2}J = J_0/2n^3, \qquad (10)$$
$$J_g = 2J = 2J_0/n^3.$$

The constant J_0 is proportional to the atomic exchange constant and should, on very general grounds, be negative. This would cause an exchange splitting between a spin singlet and a spin triplet, with the triplet lying below the singlet (Hund's rule).

The ortho and para yellow excitons are *not* triplet and singlet spin states, however, as can be readily seen from the eigenfunctions in Table VI.

The singlet Γ_2 paraexciton is pure spin triplet, while the triplet Γ_5 orthoexciton is mixed spin singlet and triplet, as noted by Kuwabara *et al.*[14] Consequently, the exchange splitting produced by negative J puts the singlet *below* the triplet in the unstressed crystal by

$$E_{\text{triplet}} - E_{\text{singlet}}(X=0) = -\tfrac{1}{6}J_y - \frac{8}{9}\frac{J^2}{\Delta'} - \tfrac{1}{2}J_y$$
$$= -\tfrac{2}{3}J_y - \frac{8}{9}\frac{J^2}{\Delta'} = -\frac{J}{3} - \frac{8}{9}\frac{J^2}{\Delta'}$$
$$= \tfrac{1}{3}|J| - \frac{8}{9}\frac{J^2}{\Delta'},$$

in agreement with recent experimental observations of the singlet $1S$ paraexciton approximately 100 cm^{-1} *below* the $1S$ triplet by Kreingold and Makarov,[12] Merle and Robino,[13] and Kuwabara, Tanaka, and Fukutani.[14]

The nonlinear least-squares analysis described above was applied to the data for the $1S$ state as follows. The parameters Δ', J, e, and h were initialized and the program proceeded to compute eigenvalues of the energy matrix (for a given stress), compare the eigenvalues corresponding to the $1S$ yellow state to the data for the same stress, and compute the sum of the squares of the differences. The procedure was repeated for each stress corresponding to experimental data and the sum of squares of differences between the entire set of experimental values and predicted eigenvalues was generated. The program then varied the parameters, repeated the above calculation, and computed the set of parameters (Δ', J, e, h) which minimized the above sum.

The analysis was carried out for a variety of initial parameter sets. In each case it was found that the final value of Δ' differed little from the starting value. The program was run thereafter with Δ' held constant while J, e, and h were varied to produce a best fit. Successive runs of the program were conducted with different values of Δ' in order to determine its effect on the fit. The results showed that the fit became noticeably better for values of Δ' greater than 3200 cm^{-1}. Numerical results for two values of Δ' are given in Table IV including deformation potentials deduced with the help of Eq. (4).

As stated earlier, Δ' (for the $1S$ yellow exciton) can reasonably be expected to be near 600 cm^{-1}

but in any case is no greater than 1065 cm^{-1}. It is not possible to reconcile the value of Δ' resulting from the data analysis with the predictions based on our understanding of the (p states of the) exciton series in Cu_2O. Plots of the theoretical stress behavior of the 1S state for two values of Δ' are compared with the experimental data in Fig. 3.

DISCUSSION AND CONCLUSIONS

It has been seen that diagonalization of the effective Hamiltonian matrix gives only moderate agreement with the experimental results for the 1S state unless an unreasonably large value of the spin-orbit constant is used. (A similar analysis for recent experiments involving [101] stress, however, has shown that reasonable agreement between theory and experiment obtains for $\Delta' \approx 600$ cm^{-1}.[24])

We have noted the reversal in the sense of the singlet-doublet splitting between the 1S and higher states as well as an increase in the magnitude of the splitting of the 3S relative to the 1S. This effect cannot be explained unless one assumes a complicated dependence of the exchange parameter on exciton state.

The quadratic coefficient for the 3S singlet $^1\Gamma_4$ state (shown in Table IV) is of the same magnitude but of opposite sign to all components of the 1S, 3D, and 4S states. As shown in Table III, both singlet and doublet components of stress-split yellow $^3\Gamma_5$ states should have quadratic coefficients $-2e^2/\Delta'$ while the quadratic coefficient of the singlet component of the stress-split green $^3\Gamma_5$ state should be $+2e^2/\Delta'$. Thus the data suggests that the state assigned as 3S yellow may in fact be a green Γ_5 state. Further indication of this is the clear difference between the quadratic coefficients of the two components of the 3S state which is also consistent with the predictions of Table III for green $^3\Gamma_5$ excitons.

Two curious aspects of the 3D state should be noted. First, its zero-stress energy very nearly coincides with the value predicted for the 3S state by a simple quantum defect calculation.[9] Furthermore, if the theoretically predicted n^{-3} dependence of the magnitude of the stress splitting were to hold, then the splitting of the 3S state at 2 kbar (which should be 1/27 of the 1S splitting) would be approximately 3 cm^{-1}, which would not be resolved in our experiment.

It is useful to examine the deformation potentials that are derived from the analysis of the preceding section. The parameters obtained there are related to the deformation potentials a and b of Eq. (4). The results, obtained from the measured elastic compliance constants,[25] are given in Table IV for two values of Δ'. Also shown are the deformation potentials for CuCl.[26] Cu_2O and CuCl should have comparable deformation potentials since their crystal structures and valence bands (derived from Cu 3d orbitals) are similar. It is seen that the agreement is better for the case $\Delta' = 600$ cm^{-1}.

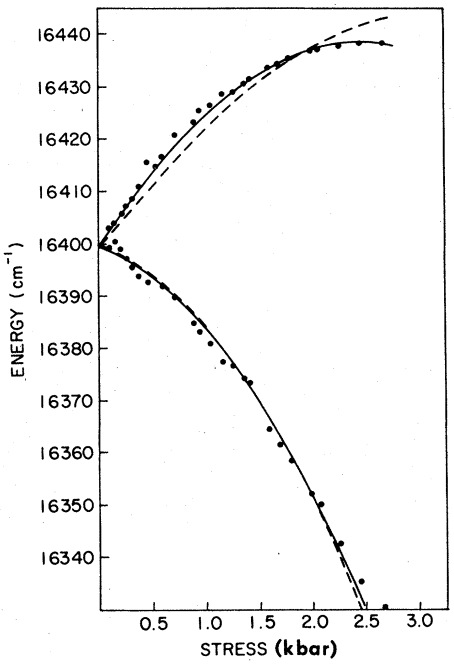

FIG. 3. Comparison of the experimental data for the 1S state with theoretical predictions resulting from diagonalization of the energy matrix (Table II). The dashed line gives the best fit that can be obtained with $\Delta' = 600$ cm^{-1} in which case $J = -150$ cm^{-1}, $e = -50$ cm^{-1} $kbar^{-1}$ and $h = 3$ $cm^{-1}kbar^{-1}$. The solid curve shows the best overall fit which obtains for $\Delta' = 3600$ cm^{-1}, $J = -357$ cm^{-1}, $e = -123$ $cm^{-1}kbar^{-1}$, and $h = 5$ $cm^{-1}kbar^{-1}$.

The limitations of the effective Hamiltonian formalism bear repeating. It was pointed out earlier that the calculation has involved only two exciton series (derived from the lowest conduction band and the two highest valence bands.) Interactions with other series have been ignored. Also, the effective Hamiltonian treats only yellow and green exciton states of a particular quantum state. Cho[19] has pointed out that the limit of applicability of this formalism may be reached if other exciton states happen to couple very strongly to the 12-fold manifold of exciton states treated in this way. In particular, if the 1S green exciton lies just below the 3S yellow, then the second-order interaction [Eq. (8)] would have negative Δ' and could produce the observed inversion in sense and large magnitude of the linear splitting of the 3S yellow. The overlap integral between the 1S green and 3S

yellow envelope functions could be large because of the very different Bohr radii of the two series. Within the framework of this explanation, it would have to be assumed that the 1*S* green exciton is much broader than its yellow counterpart in order to understand the absence of enhanced Raman scattering in the vicinity of the assumed energy of the 1*S* green. Finally, there is a stress-dependent part of the spin-orbit interaction which has not been accounted for[11] although its effect is expected to be small.

Very recently D. Fröhlich *et al.* have reported a two-photon spectroscopic investigation of Cu_2O which resolves many of the apparent inconsistencies we have described.[27] They find that the 1*S* green exciton lies just 134 cm^{-1} below the 2*S* yellow (which we have designated 3*S* yellow) and is strongly mixed with it by the exchange interaction. The mixing also results in a transfer of most of the combined oscillator strength to the 2*S* yellow exciton, which explains its strong resonant enhancement as well as the absence of observable resonant enhancement at the position of the 1*S* green. Both the large linear splitting term and the inverted quadratic term that we found for the 2*S* yellow exciton are presumably due to this mixing and can, in principle, be analyzed by extending our calculation to a 24-state basis.

ACKNOWLEDGMENTS

This work was supported by the National Science Foundation under Grants Nos. DMR74-12040, DMR77-23788, and DMR78-03030. We thank J. L. Birman and R. Elliott for useful discussions pertaining to this investigation. We are particularly grateful to Rhoda Berenson for providing us with unpublished calculations of the Raman-scattering tensors for stressed Cu_2O. Finally, we thank Richard A. Forman for providing the crystals used in this experiment.

APPENDIX: BAND AND EXCITON WAVE FUNCTIONS

We have the following tables:

TABLE V. Zone-center Bloch functions (Valence band). From Koster *et al.* Table 83 ($Y'' \equiv Y_2^{-2} - Y_2^2$).

$$\Psi^{\Gamma_7}_{+1/2} = -\frac{i}{\sqrt{3}}[xy\alpha + (yz + ixz)\beta] = \frac{-1}{\sqrt{6}}(Y''\alpha + 2Y_2^{-1}\beta)$$

$$\Psi^{\Gamma_7}_{-1/2} = -\frac{i}{\sqrt{3}}[-xy\beta + (yz - ixz)\alpha] = \frac{1}{\sqrt{6}}(Y''\beta - 2Y_2^{1}\alpha)$$

$$\Psi^{\Gamma_8}_{+3/2} = \frac{i}{\sqrt{6}}[2xy\beta + (yz - ixz)\alpha] = \frac{1}{\sqrt{3}}(Y''\beta + Y_2^{1}\alpha)$$

$$\Psi^{\Gamma_8}_{+1/2} = -\frac{i}{\sqrt{2}}[(yz - ixz)\beta] = -Y_2^{1}\beta$$

$$\Psi^{\Gamma_8}_{-1/2} = \frac{i}{\sqrt{2}}[(yz + ixz)\alpha] = Y_2^{-1}\alpha$$

$$\Psi^{\Gamma_8}_{-3/2} = \frac{i}{\sqrt{6}}[2xy\alpha - (yz + ixz)\beta] = \frac{1}{\sqrt{3}}(Y''\alpha - Y_2^{-1}\beta)$$

TABLE VI. Wave functions and energies of the 4 yellow and 8 green exciton states with orbital quantum numbers n including Coulomb and spin-orbit interactions.

No.	Exciton	Symmetry	Wave function	Energy E^0
ϕ_{12}	Singlet Yellow Γ_2 (paraexciton)	Ψ^{Γ_2}	$\Phi_{yn}\left(\frac{1}{\sqrt{12}}\right)[Y''(\alpha\beta_c + \beta\alpha_c) + 2Y_2^{-1}\beta\beta_c - 2Y_2^{1}\alpha\alpha_c]$	E_c^{yn}
ϕ_5	Triplet	$\Psi^{\Gamma_5}_{yz}$	$\Phi_{yn}\left(-\frac{i}{\sqrt{12}}\right)[Y''(\alpha\alpha_c + \beta\beta_c) + 2Y_2^{-1}\beta\alpha_c - 2Y_2^{1}\alpha\beta_c]$	E_c^{yn}
ϕ_8	Yellow $^3\Gamma_5$ (orthoexciton)	$\Psi^{\Gamma_5}_{xz}$	$\Phi_{yn}\left(\frac{1}{\sqrt{12}}\right)[Y''(\beta\beta_c - \alpha\alpha_c) - 2Y_2^{1}\alpha\beta_c - 2Y_2^{-1}\beta\alpha_c]$	E_c^{yn}
ϕ_{10}		$\Psi^{\Gamma_5}_{xy}$	$\Phi_{yn}\left(-\frac{i}{\sqrt{12}}\right)[Y''(\beta\alpha_c - \alpha\beta_c) - 2Y_2^{1}\alpha\alpha_c - 2Y_2^{-1}\beta\beta_c]$	E_c^{yn}
ϕ_3	Triplet	$\Psi_x^{\Gamma_4}$	$\Phi_{gn}\left(\frac{i}{\sqrt{8}}\right)[Y''(\alpha\alpha_c + \beta\beta_c) + Y_2^{1}(\alpha\beta_c + \beta\alpha_c) - Y_2^{-1}(\beta\alpha_c + \alpha\beta_c)]$	$\Delta + E_c^{gn}$
ϕ_6	Green	$\Psi_y^{\Gamma_4}$	$\Phi_{gn}\left(\frac{1}{\sqrt{8}}\right)[Y''(\beta\beta_c - \alpha\alpha_c) + Y_2^{1}(\beta\alpha_c + \alpha\beta_c) + Y_2^{-1}(\beta\alpha_c + \alpha\beta_c)]$	$\Delta + E_c^{gn}$
ϕ_1	$^3\Gamma_4$	$\Psi_z^{\Gamma_4}$	$\Phi_{gn}\left(\frac{i}{\sqrt{2}}\right)(Y_2^{-1}\alpha\alpha_c + Y_2^{1}\beta\beta_c)$	$\Delta + E_c^{gn}$

Table VI. *(Continued.)*

No.	Exciton	Symmetry	Wave function	Energy E^0
ϕ_2	Doublet	$\Psi_1^{\Gamma_3}$	$\Phi_{gn}\left(\frac{-1}{\sqrt{2}}\right)(Y_2^{-1}\alpha\alpha_c - Y_2^1\beta\beta_c)$	$\Delta + E_c^{gn}$
ϕ_{11}	Green $^2\Gamma_3$	$\Psi_2^{\Gamma_3}$	$\Phi_{gn}\left(\frac{-1}{\sqrt{6}}\right)[Y''(\alpha\beta_c + \beta\alpha_c) + Y_2^1\alpha\alpha_c - Y_2^{-1}\beta\beta_c]$	$\Delta + E_c^{gn}$
ϕ_4	Triplet	$\Psi_{yz}^{\Gamma_5}$	$\Phi_{gn}\left(\frac{-i}{\sqrt{24}}\right)[Y''(\alpha\alpha_c + \beta\beta_c) + 3(Y_2^{-1}\alpha\beta_c - Y_2^1\beta\alpha_c) + Y_2^1\alpha\beta_c - Y_2^{-1}\beta\alpha_c]$	$\Delta + E_c^{gn}$
ϕ_7	Green $^3\Gamma_5$	$\Psi_{xz}^{\Gamma_5}$	$\Phi_{gn}\left(\frac{1}{\sqrt{24}}\right)[Y''(\beta\beta_c - \alpha\alpha_c) - 3(Y_2^{-1}\alpha\beta_c + Y_2^1\beta\alpha_c) + Y_2^{-1}\beta\alpha_c + Y_2^1\alpha\beta_c]$	$\Delta + E_c^{gn}$
ϕ_9		$\Psi_{xy}^{\Gamma_5}$	$\Phi_{gn}\left(\frac{1}{\sqrt{6}}\right)[Y''(\beta\alpha_c - \alpha\beta_c) + Y_2^1\alpha\alpha_c + Y_2^{-1}\beta\beta_c]$	$\Delta + E_c^{gn}$

*Present address: Optical Information Systems, Elmsford, N. Y. 10523.

†Present address: Perkin Elmer Corporation, Norwalk, Connecticut 06856.

[1]M. Hayashi and K. Katsuki, J. Phys. Soc. Jpn. 5, 381 (1950).

[2]E. F. Gross and A. A. Kaplyanskii, Fiz. Tverd. Tela. 2, 379 (1960) [Sov. Phys. Solid State 2, 353 (1960)].

[3]J. L. Diess and A. Daunois, Surf. Sci. 37, 804 (1973); S. Nikitine, in *Optical Properties of Solids*, edited by S. Nudelman and S. S. Mitra (Plenum, New York, 1969), p. 214 ff.

[4]A. Daunois, J. L. Diess, J. C. Merle, C. Wecker and S. Nikitine, in *Eleventh International Conference on the Physics of Semiconductors, Warsaw, 1972* (State Publishing House, Warsaw, 1973), p. 1402.

[5]E. F. Gross and A. A. Kaplyanskii, Fiz. Tverd. Tela. 2, 2968 (1960) [Sov. Phys. Solid State 2, 2637 (1961)].

[6]R. J. Elliott, Phys. Rev. 124, 340 (1961).

[7]V. T. Agekyan, E. F. Gross, and A. A. Kaplyanskii, Fiz. Tverd. Tela. 7, 781 (1965) [Sov. Phys. Solid State 7, 623 (1965)].

[8]V. T. Agekyan and Yu. A. Stepanov, Fiz. Tverd. Tela. 17, 1592 (1975) [Sov. Phys. Solid State 17, 1041 (1975)].

[9]M. A. Washington, A. Z. Genack, H. Z. Cummins, R. H. Bruce, A. Compaan, and R. A. Forman, Phys. Rev. B 15, 2145 (1977).

[10]W. S. Brower, Jr. and H. S. Parker, J. Cryst. Growth 8, 227 (1971).

[11]F. H. Pollak, Surf. Sci. 37, 863 (1973) and references therein.

[12]F. I. Kreingold and V. L. Makarov, Fiz. Tekh. Poluprovodn. 8, 1475 (1974) [Sov. Phys. Semicond. 8, 962 (1975)].

[13]J. C. Merle and M. Robino, Opt. Commun. 14, 240 (1975).

[14]G. Kuwabara, M. Tanaka, and H. Fukutani, Solid State Commun. 21, 599 (1977).

[15]R. Berenson (unpublished).

[16]Joseph L. Birman, Phys. Rev. B 9, 4518 (1974).

[17]V. A. Kiselev and A. G. Zhilich, Fiz. Tverd. Tela. 13, 2398 (1971) [Sov. Phys. Solid State 13, 2008 (1972)].

[18]D. W. Langer, R. N. Euwema, K. Era, and T. Koda, Phys. Rev. B 2, 4005 (1970).

[19]K. Cho, Phys. Rev. B 14, 4463 (1976).

[20]G. E. Pikus, Fiz. Tverd. Tela. 6, 324 (1964) [Sov. Phys. Solid State 6, 261 (1964)].

[21]G. F. Koster, J. O. Dimmock, R. G. Wheeler, and H. Statz, *Properties of the Thirty-Two Point Groups* (M.I.T. Press, Cambridge, MA, 1963).

[22]J. C. Slater, *The Quantum Theory of Molecules and Solids* (McGraw-Hill, New York, 1960), Vol. II, p. 519.

[23]M. Cardona, *Modulation Spectroscopy*, Solid State Phys., Suppl. No. 11 (Academic, New York, 1969).

[24]R. G. Waters (unpublished).

[25]M. H. Manghani, W. S. Brower, and H. S. Parker, Phys. Status Solidi A 25, 69 (1974).

[26]T. Koda, T. Murahashi, T. Mitani, S. Sakoda, and Y. Onodera, Phys. Rev. B 5, 705 (1972).

[27]D. Fröhlich, R. Kenklies, Ch. Uihlein, and C. Schwab, Phys. Rev. Lett. 43, 1260 (1979).